

## Plasma MHD Stability at Limiting Density on Globus-M.

Yu.V.Petrov<sup>1</sup>, V.K.Gusev<sup>1</sup>, S.V.Krikunov<sup>1</sup>, G.S.Kurskiev<sup>1</sup>, R.G.Levin<sup>1</sup>, V.B.Minaev<sup>1</sup>,  
M.I.Patrov<sup>1</sup>, N.V.Sakharov<sup>1</sup>, S.Yu.Tolstyakov<sup>1</sup>, V.I.Varfolomeev<sup>1</sup>, S.E.Bender<sup>2</sup>,  
E.G.Kuzmin<sup>2</sup>, I.A.Mironov<sup>2</sup>

<sup>1</sup> *A.F.Ioffe Physico-Technical Institute, St.Petersburg, Russia*

<sup>2</sup> *D.V. Efremov Institute of Electrophysical Apparatus*

During the last year experiments on Globus-M (major radius 0.36 m, minor radius 0.24 m) were continued at densities close to the Greenwald limit. The experiments were carried out at toroidal magnetic field 0.4 T, plasma currents in the range of 150-250 kA, in OH regime and at auxiliary heating by means of NBI, in limiter and diverter configurations. In contrast to our previous experiments [1], the plasma current degradation at high density was prevented by a feedback stabilization system, permitting to emphasize the effect of the density rise on the plasma stability. The main diagnostics for mode identification were a multi-channel SXR pinhole camera and a set of 44 Mirnov coils [2]. The plasma density and temperature profiles were measured by Thomson scattering. The operating range of the

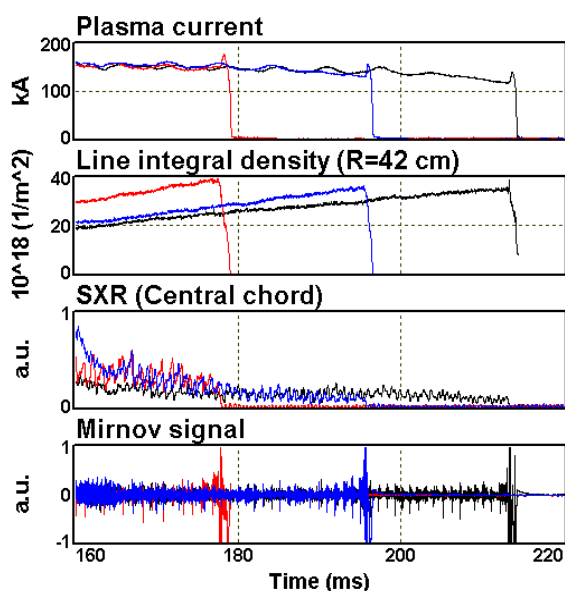


Fig.1 Density limit approach at three different gas puff rates: slow (shot #16159, black traces), middle (shot #16186, blue traces) and fast (shot #16173, red traces). The plasma breakdown is at 113 ms.

microwave interferometer was enhanced by decreasing the probing wave length from 1.2 to 0.8 mm, which provided measurements at all plasma densities practically approached in Globus-M.

Three piezoelectric valves were used for gas puffing. Two of them are installed on upper and lower domes of the tokamak from the low magnetic field side and the third in equatorial plane from the high field side. The experiments have demonstrated, that gas puff effectiveness does not depend on the valve position. The simultaneous operating of two valves does not increase effectiveness also, and density rise rate is

only determined by the total gas flow. Fig.1 shows the limit density approach at three different gas puff rates: from minimal (shot #16159) to maximum one (shot #16173). It is seen from the figure that the density reaches approximately the same value, but for different time. High density shots are characterized by the low MHD activity level, that is confirmed by Mirnov signals, shown in the figure. Generally, the only essential observed instability were sawtooth oscillations, registered by the SXR camera. The highest amplitude of the sawtooth oscillations were in the shots with faster density increase. It may be explained by sharper electron density profile in these discharges, arising due to the periphery cooling with

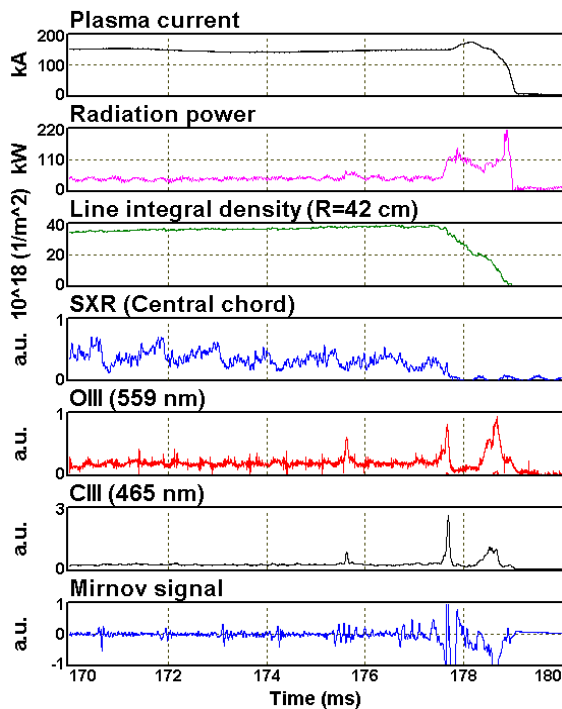


Fig.2. Waveforms demonstrating radiation collapse at limit density in OH shot #16173

radiation collapse scenario: fast periphery cooling, impurity radiation rise, recorded by a bolometer and spectrometer on OIII and CIII lines (see Fig.2), and, at last, magnetic reconnection leading to disruption.

Other instability observed in high density discharges is internal mode  $m=1/n=1$ , ‘snake’, which coupling with external  $m=2/n=1$  mode may lead to disruption (that frequently occurred in our earlier experiments [3]). However, this phenomenon is not observed at clean enough tokamak walls. The mode  $m=2/n=1$  arising in the beginning of a discharge is suppressed with saw-tooth oscillation grow, and the mode  $m=1/n=1$  development does not lead to any essential consequences. Fig.3 demonstrates evolution of the ‘snake’ instability in

intensive gas flow, and hence sharper current density profile. This assumption is supported by electron temperature profiles  $T_e(r)$  measured by means of Thomson scattering and safety factor  $q(r)$  profiles reconstructed with equilibrium code EFIT. However, the saw-tooth oscillations seemed not to restrict the density rise, as their magnitude did not effect the value of the Greenwald parameter,  $\langle n \rangle / n_{GW}$ , which approached 0.9 value in OH experiments on Globus-M. The Greenwald density here is defined by the formula:

$$n_{GW}(10^{20} \text{ m}^{-3}) = I_p(\text{MA}) / \pi a^2(\text{m}).$$

On exceeding this limit, a discharge is terminated by disruption according with

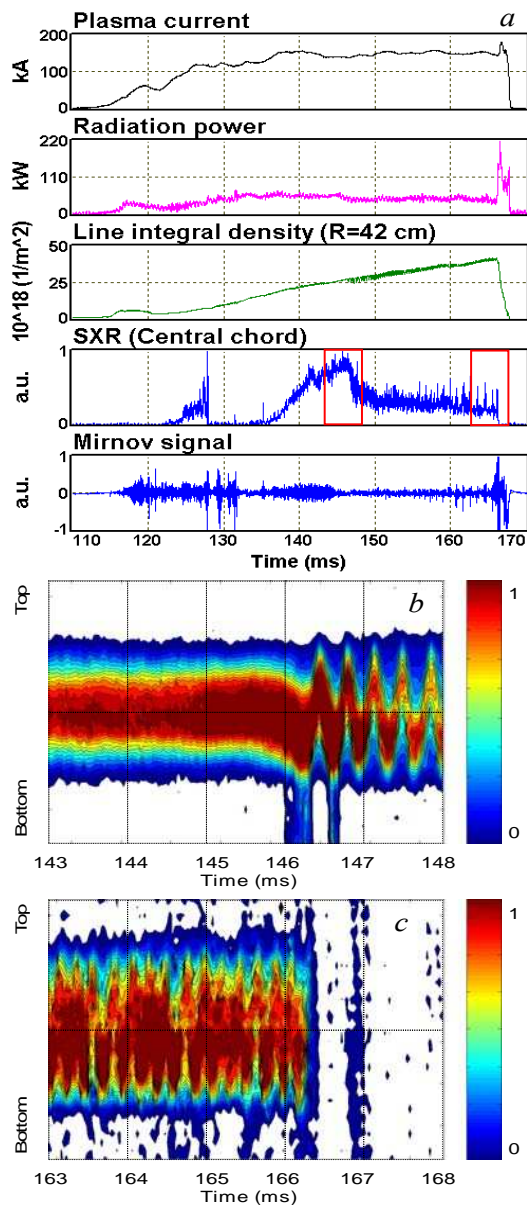


Fig.3 a-waveforms of the high density shot #15945 with snake (142-165 ms), b-start of the snake observing with SXR pinhole camera, c-saturated snake at the end of the shot

shot #15945 with limit plasma density. The Greenwald parameter in this shot reaches value 0.9, as in the best shorts with saw-tooth oscillations. On the traces of the microwave interferometer and SXR signal one can see the snake appearing at 142 ms and existing to the end of the discharge. The start of the snake is clearly seen in intensity diagram of the SXR pinhole camera signal (Fig.3b). In Fig.3c, it is seen the snake in saturated condition, existing up to the discharge termination at 165 ms. It is worth to notice that the appearing of snake, itself, has begun rather chance, than regularity in discharges with a density close to the limit.

Attempts to exceed the Greenwald limit were carried out at auxiliary heating by means of the neutral beam co-injection with energy from 22 to 28 keV and power of 300-500 kW. The implementation of NBI has allowed us to extend the density limit in absolute value  $\langle n \rangle$  from  $0.9 \times 10^{20}$  to  $1.1 \times 10^{20} \text{ m}^{-3}$ , but has not increased the Greenwald parameter. The points in

Hugill diagram corresponding to NBI shorts (blue rectangles in Fig.4) are placed righter than the points corresponding to OH shots (red circles in Fig.4), but the maximum  $\langle n \rangle / n_{GW}$  ratio is the same  $\sim 1$  inside the measurement errors of 10%. The following explanation of this fact may be done. The easier way to approach the Greenwald limit is operating at lower plasma currents and, hence, higher  $q(a)$ . It was realized in OH shots, and the Greenwald parameter  $\sim 1$  has been achieved at the plasma currents 130-150 kA. But NBI is not effective at such currents because the poor confinement of energetic ions. Increase of the plasma current up to

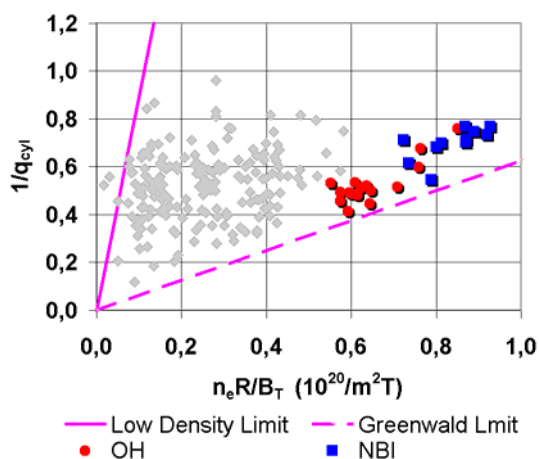


Fig.4 Hugill diagram for Globus-M shots. Colored points correspond to the last year high density experiments

200-250 kA leads to weaker MHD stability due to lower  $q(a)$ , and these OH shorts suffer from internal reconnection events (IRE). The problem can be solved by increase the toroidal field, which is possible in future, but needs some upgrade of the toroidal field coils.

Implementation of the NBI permits achievement of higher plasma density, due to additional power, obtaining for ionization and heating of the neutral gas incoming from the gas puffing, which stabilizes IREs. As a result, the density achieved at NBI was by 20% higher as compared with OH shots at the same other conditions. Such modest enhancement of the limit density corresponds to the scaling obtained on ASDEX [4], which defines that limit density  $n_{lim} \sim P_{in}^{0.25-0.4}$ , where  $P_{in}$  – incoming power. So, in our case the incoming power in OH regime (about 400-500 kW) is doubled at NBI (up to 500 kW), which leads to 20-30 % -increase of the density limit in accordance with the scaling. Further increase of the limit is possible at higher NBI power that can be realized with a new more powerful ion source, which is under preparation now.

### Conclusions

High density, approaching the Greenwald limit has been realized in Globus-M in OH and NBI shots. The snake and sawtooth instabilities, observed in these experiments seem not to affect the density limit, and the thermal imbalance between input power and radiation losses looks like the only reason for disruption. The attempts to overcome the limit will be continue at higher toroidal fields and NBI power.

*The work is supported by Russian Academy of Sciences, Ministry of Education and Science of RF, Rosatom of RF, IAEA Research Contract No 12408 and RFBR grants 05-02-17773, 05-08-18044, 06-02-16709.*

### References

1. V.K. Gusev et al, (Proc. 32<sup>nd</sup> EPS Plasma Phys. Conf. Tarragona 2005) ECA, 29C P5-076
2. Yu.V. Petrov et al, (Proc. 3<sup>d</sup> IAEA TM on ST, St.Petersburg 2005) CDROM, OV-4
3. V.K. Gusev et al, (Proc. 31<sup>st</sup> EPS Plasma Phys. Conf. London 2004) ECA, 28G P4-158
4. Stäbler A. et al, Nucl. Fusion 32 (1992) 1557.